KSCE Journal of Civil Engineering (2018) 22(9):3663-3675

DOI 10.1007/s12205-018-1357-z

Tunnel Engineering

pISSN 1226-7988, eISSN 1976-3808
www.springer.com/12205

Risky Ground Prediction ahead of Mechanized Tunnel Face using Electrical Methods: Laboratory Tests

Jinho Park*, Jinwoo Ryu, Hangseok Choi***, and In-Mo Lee******

Received September 18, 2017/Revised November 13, 2017/Accepted December 3, 2017/Published Online March 2, 2018

Abstract

An accurate determination of the ground condition ahead of a tunnel face is key to stable excavation of tunnels using a Tunnel Boring Machine (TBM). This study verifies the effectiveness of using the Induced Polarization (IP) method along with electrical resistivity for identifying hazardous ground conditions ahead of a tunnel face. The advancement of the TBM toward a fault zone, seawater bearing zone, soil-to-rock transition zone, and mixed-ground zone is artificially modeled in laboratory-scale experiments. The IP and resistivity are assumed to be measured at the tunnel face, whenever the excavation is stopped to assemble one ring of a segmental lining. The measured IP showed completely different trends from the measured resistivity and varies with the type of hazardous zone. As the TBM approached the fault zone, transition zone, and mixed ground, the IP values were observed to be constant, increasing, and fluctuating, respectively. Therefore, a more reliable prediction of the ground condition ahead of a tunnel face can be achieved by using the IP and resistivity methods together. A table that can be used to predict the ground conditions based on the afore-mentioned methods is presented in this paper for use in mechanized tunneling job sites.

Keywords: *tunnel boring machine, ground condition, induced polarization, electrical resistivity, tunnel face*

1. Introduction

Generally, mechanized tunnel excavation using a Tunnel Boring Machine (TBM) offers a safer work environment during tunnel construction, as compared to excavation using drilling and the blasting method. However, even in TBM tunneling job sites, many potential risks still exist that can degrade the safety of tunnels and/or reduce the efficiency of tunnel excavation. And among the potential risks, more than 85% of the risks arise because of geological factors (Chang *et al.*, 2006); hence, hazardous geological conditions are the most problematic factors in mechanized tunneling jobs.

Thus, at the design stage of the tunneling work, a geotechnical investigation is performed on the ground surface by drilling boreholes and by performing geophysical explorations along the tunnel route. Nevertheless, if a TBM runs relying on geological profiles containing surface-investigated ground conditions, it could frequently encounter unexpected changes in ground conditions during tunnel construction. In other words, the surface-explored geological profiles present only the overall geological structure, which is not an accurate representation of the actual ground conditions. Therefore, as an alternative, ground condition prediction methods that can be implemented inside the tunnel during excavation are developed to provide more reliable ground information. Moreover, the demand for a comprehensive and prompt prediction of the ground conditions ahead of a tunnel face has led to the development of non-destructive geophysical exploratory techniques such as the tunnel seismic prediction (Dickmann and Sander, 1996), ground penetrating radar (Grodner, 2001), electromagnetic exploration (McDowell *et al.*, 2002), and tunnel resistivity prediction (Cho *et al.*, 2005; Park *et al.*, 2016).

Among the various non-destructive methods, the combined method of the electrical resistivity and Induced Polarization (IP) has been developed. The bore-tunneling electrical ahead monitoring (BEAM) (Kaus and Boening, 2008) system was developed for ground prediction by measuring the resistivity and IP of the ground. The BEAM system suggested a matrix for identifying ground conditions based on the measured resistivity and IP values. A low IP value implies a high degree of fractures in the rock. However, in a recent study for evaluating the effectiveness of the IP for identifying fractured rocks/soft ground conditions (Park *et al.*, 2017b) it was verified that the IP is mostly controlled by the size of the narrow pores within the ground rather than by the fracture characteristics.

*Research Professor (Research Associate, University of California, Berkeley, CA 94720, Unites States), School of Civil, Environmental, and Architectural Engineering, Korea University, Seoul 02841, Korea (E-mail: smpjh7@korea.ac.kr)
**Graduate Student, School of Civil, Environmental and Architectural Engineering, Korea University, Seoul 02841, Korea (E-mail: nike@korea.ac.kr)
***Member, Professor, School of Civil, Environmental and Architectural Engineering, Korea University, Seoul 02841, Korea (E-mail: hchoi2@korea.ac.kr)
****Member, Professor, School of Civil, Environmental and Architectural Engineering, Korea University, Seoul 02841, Korea (Corresponding Author, E-mail: inmolee@korea.ac.kr)

On the other hand, as the demand for sensing techniques based on electrical properties applicable to TBMs increases, various methods for installing or integrating electrodes on the TBMs are being developed. In the BEAM system, electrodes are fixed on electrically insulated disc cutters and on the tail seal. However, these electrodes are unsafe because the excavated muck is likely to damage them. Therefore, the use of disc cutters themselves as electrodes or electrodes installed on the segmental lining is proposed for measuring the resistivity of the ground ahead of the tunnel face (Robert, 2014).

The aim of this study is to propose a new method for predicting risky ground conditions ahead of the mechanized-tunneling face using the combined method of the resistivity and IP, as a further development of the prediction method using only a resistivity method which can identify a vertical anomalous zone ahead of the tunnel face (refer to Park *et al.*, 2017a). The new method has following novelties:

The advantages of using the IP along with the resistivity are newly proposed for identifying the major types of hazardous ground conditions in mechanized-tunnelling job sites. A table that can be used to predict the risky ground types based on the observed resistivity and IP values together is provided for use in TBM sites.

The new method uses four-electrode installed on the cutter-head and the resistivity and IP can be measured together whenever the excavation is stopped to assemble one ring of a segmental lining. Therefore, the method is highly practical and effective to mechanized-tunnelling job sites without any hinderance to construction process using a TBM.

In the laboratory-scale experiments, advancement of the TBM toward a fault zone, seawater bearing zone, soil-to-rock transition zone, and mixed-ground zone was artificially simulated. The trend of changes in the measured resistivity and IP was observed at the tunnel face during excavation.

2. Background

2.1 Electrical Resistivity Survey

The electrical resistivity of the ground in a saturated condition is controlled by the porosity of the rock and the resistivity of the pore water. The resistivity of the saturated rock (ρ_{rock})(Ωm) can be expressed as follows (Archie, 1942):

$$\rho_{rock} = \rho_w \cdot n^{-\theta} \tag{1}$$

where ρ_w is the resistivity of the pore water (Ωm), n is the porosity, and θ is the shape factor that generally ranges from 1.3 to 2.5 (n and θ are dimensionless). The resistivity of a rock will decrease when the rock is saturated with water and/or when the rock has a high pore volume because of fracturing. Additionally, rocks with high strength generally tend to have a high density and low porosity, resulting in a high electrical resistivity (Morrow *et al.*, 2015).

It is assumed that four electrodes are installed linearly in the cutter head as shown in Fig. 1: A, M, N, and B. An electric current (I) (A) is injected between electrodes A and B, and the resulting electric potential (ΔV) (V) is measured between electrodes M and N. Electrical resistance (R) (Ω) is defined by Ohm's law ($R = DV/I$). The electrical resistivity (ρ) (Ωm) is then calculated as (Reynolds, 1997):

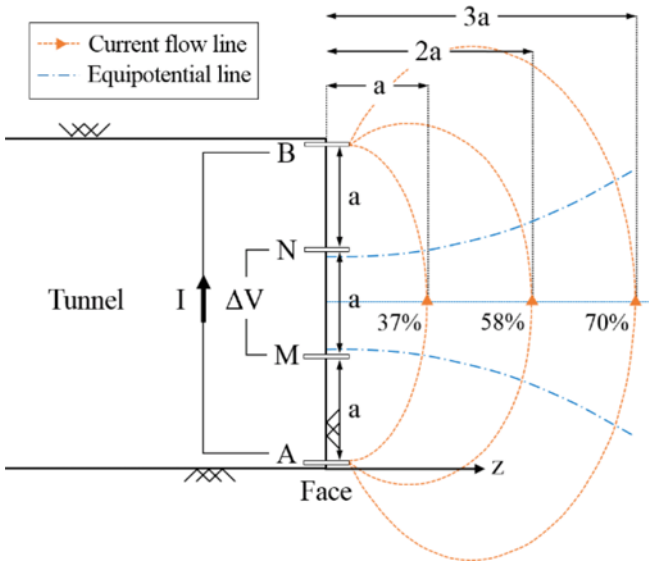

Fig. 1. Four-electrode Resistivity Prediction in a Tunnel Using a Wenner Array

$$\rho = K \cdot R = 2\pi\left(\frac{1}{AM} - \frac{1}{MB} - \frac{1}{AN} + \frac{1}{NB}\right)^{-1} \cdot \frac{\Delta V}{I} \tag{2}$$

where K is a geometrical coefficient (m) that depends on the arrangement of the four electrodes A, M, N, and B. AM, MB, AN, and NB represent the geometrical distance (m) between the electrodes A and M, M and B, A and N, and N and B, respectively. There are several electrode arrays such as Wenner, Schlumberger, Pole-Pole, and Dipole-Dipole, which are defined by the relative spacing and position of the four electrodes. Meanwhile, Fig. 1 illustrates a Wenner electrode array installed on the tunnel face with equal electrode spacings of a.

Figure 1 shows each current flow line introduced into the homogeneous ground ahead of the tunnel face. Each current flow line shows a percentage of the total injected current passing within that particular line (Schaeffer and Mooney, 2016). For example, the 58% current flow line indicates that 58% of the total current flows within this line. Fig. 1 indicates that as the depth increases (z = a, 2a, 3a…), the percentage of current increases, and will reach 100% at infinite depth ($z \rightarrow \infty$) (Schaeffer and Mooney, 2016). In addition, as the spacing of the current electrodes (AB = 3a) increases, the flow line indicating a certain percentage will get deeper into the ground in front of the tunnel face, which means that the exploration depth will increase as the diameter of a tunnel increases, so that the electrodes can be installed with a wider electrode spacing.

2.2 Time-domain IP in the Ground

In the time-domain IP method, the direct electric current that

flows into the ground is abruptly turned off. The attenuating voltage is then measured for a given time to estimate the apparent chargeability, so that the polarization characteristics of the ground can be determined. The electric potential difference created between the potential electrodes does not abruptly disappear once the current is turned off but starts to decrease slowly, which is a phenomenon that occurs from the resultant voltage caused by the accumulated cations inside the ground (Park *et al.*, 2017b). Therefore, the measured IP value can be used to identify the ground condition, as the number of accumulated cations can vary depending on the ground condition. From Fig. 2, the chargeability (m) (milliseconds) that represents the polarization characteristics can be expressed as

$$m = \frac{1}{V_0}\int_{t_1}^{t_2} V(t)dt \tag{3}$$

The chargeability can also be presented as a dimensionless form by additionally dividing the chargeability (m) (estimated by using Eq. (3)) by the time window ($t_2 - t_1$). The relationship between the chargeability (denoted as m) and the variables affecting the chargeability was proposed for the condition where circular sand particles of identical size are densely packed, and is expressed as follows (Fig. 3):

$$m = \frac{4\delta^2\left(\frac{1}{r_2}-\frac{1}{r_1}\right)^2}{\frac{r_1}{r_2}+\frac{1}{\alpha}\left(\frac{r_2}{r_1}+1\right)+1} \tag{4}$$

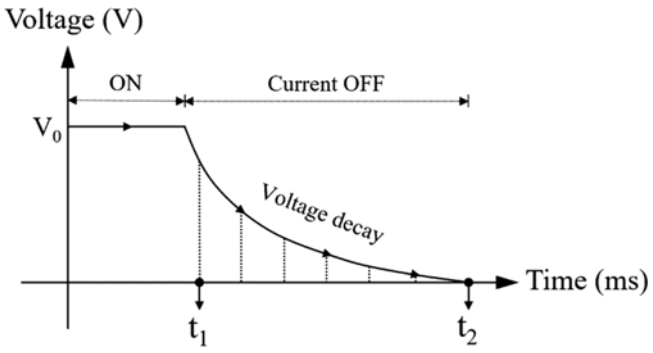

Fig. 2. Voltage Decay Curve in the Time Domain IP

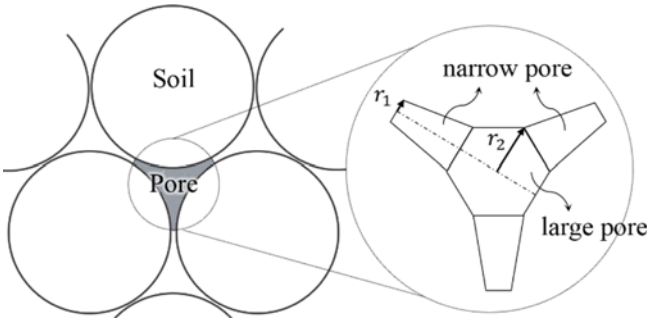

Fig. 3. Conceptual Pore Model: Inducing Chargeability in Water-saturated Ground

where r_1 and r_2 represent the radius (m) of narrow and large pores, respectively, as shown in Fig. 3, and δ represents the Debye length or the thickness (m) of the electrical double layer, which is inversely proportional to the square root of the pore water concentration (C_0) (mol/m^3) ($\delta \propto 1/\sqrt{C_0}$). The coefficient of efficiency of narrow pores is denoted by α (dimensionless) and is dependent on the surface conductivity.

On the other hand, the radius of the narrow pore (r_1) between particles, where current passes through, is the most influential factor affecting the chargeability followed by the concentration of pore water (C_0) (Park *et al.*, 2017b). As the radius of the narrow pore (r_1) decreases, the electrical double layer effect increases, resulting in an increase in chargeability (Titov *et al.*, 2004). Further, when the salinity of the pore water (C_0) increases, the thickness of the electrical double layer (δ) decreases, which in turn leads to a decrease in chargeability (refer to Eq. (4)). However, it should be noted that if one influential factor varies, it may simultaneously result in variations of other influential factors on the IP. Therefore, a more advanced sensitivity analysis, considering multi-variations in influential factors, may provide a more quantitative and reliable sensitivity analysis results to determine the key influencing factors on the IP (Vu-Bac *et al.*, 2016). On the other hand, the results show that the chargeability is not sensitive to the variation in the other two variables (the coefficient of efficiency of narrow pores (α) and the radius of the large pore (r_2)).

3. Influence of Risky Ground Conditions on Mechanized Tunneling

Among the various risks that hinder tunneling work using a TBM, the risks presented by unexpected geological changes constitute the majority of all the potential risks. They can lead to large-scale accidents during tunneling work. In this section, problematic geological conditions and how they cause damage during mechanized tunneling work are described. In the end, the hazardous ground conditions that essentially need to be predicted and identified in the early stages are discussed.

3.1 Jointed or Fault Zones

A fractured zone having joints and/or faults within a rock is created by brittle deformation of the rock when subject to high pressure (under low temperature conditions) in the shallow crust of the earth. Fractures exhibiting no or minimal relative displacement between rocks are called joints; in contrast, the existence of relative displacement indicates faults. A fault zone can range from a few millimeters to hundreds of meters. Among the various hazardous ground conditions that are encountered during TBM tunneling (see Fig. 4), fracture zones can cause the most severe problems. First, excessive ground settlement or even the collapse of the ground is likely to occur when a TBM drives through fracture zones, and such ground movement can confine the machine, resulting in the so-called TBM jamming. Countermeasures such as moving the TBM backward and injecting grouts into the loosened ground involve high costs and a long TBM downtime. In addition,

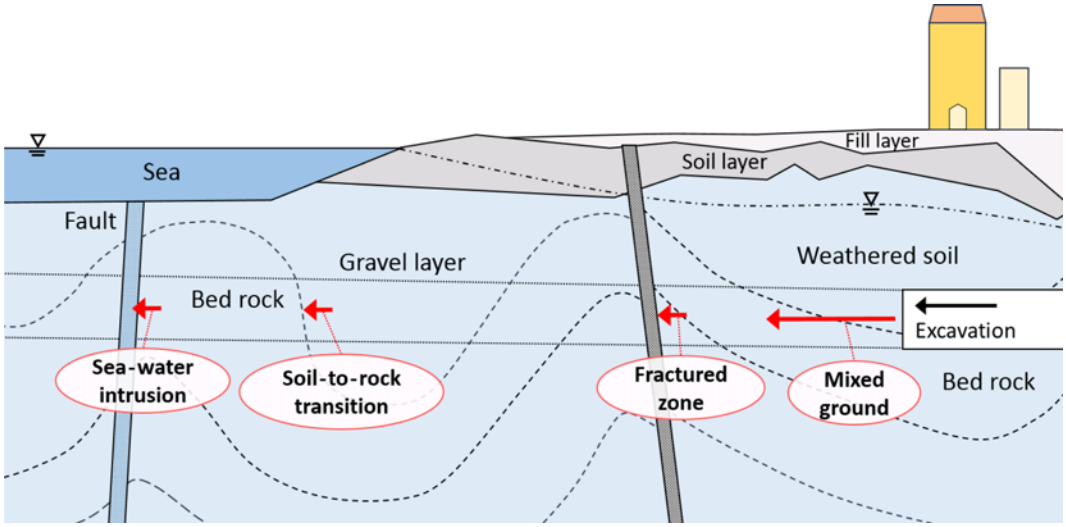

Fig. 4. Hazardous Ground Conditions on TBM Tunneling

water inflow into the tunnel face through the highly permeable fracture zone causes difficulties during TBM operations. Inflowing water presents the potential risk of ground collapse, resulting in an unsafe working environment. Thus, predicting fracture zones in advance by injecting grouts into the fracture zone ahead of the tunnel face enables engineers to be prepared for accidents.

3.2 Seawater-bearing Zones

In subsea or urban tunneling environments, limited surface investigation increases the potential risk of unexpected water inflow at the tunnel face. In particular, when the TBM drives below coastal areas or sea beds, the inflow of salty water can cause malfunctioning of the TBM and facilitate the corrosion of tunnel structures. Salty water can also render the function of backfilled grout invalid by hindering grout hardening. Moreover, the inflow of enormous amounts of water induced by high water pressure can degrade the entire safety of the tunnel and devastate the work environment. At the Great Belt tunnel in Denmark, seawater inflow led to the immersion of the tunnel and collapse of the ground. The restoration of the tunnel delayed the construction by two years, which led to an additional cost amounting to 50% of the total construction cost (Vlasov *et al.*, 2001). Therefore, predicting poor ground, where seawater can intrude, in advance is vital for tunneling work in coastal urban areas or under the sea. Pre-injection of grout into sea water intruded ground or installation of cofferdams or waterways can be performed as precautionary measures if engineers manage to detect seawater-bearing zones ahead of a TBM.

3.3 Soil-to-rock Transition Zones

The installation of suitable cutting tools on the cutter head greatly affects the efficiency of TBM excavation. Bit-type cutters, which penetrate the tunnel face ground with shallow depth and generate low TBM torque, are adequate for scraping the soil. Disc-type cutters, on the other hand, which penetrate relatively deeper into the tunnel face, are adequate for chipping away rocks with a higher torque. Therefore, the sudden emergence of steep hard rock during the excavation of soil, with the cutter head rotating at a high speed, can affect the rotating bit and disc cutters. Broken cutters lower the efficiency of ground excavation and increase construction time, because the broken cutters have to be replaced, which requires stopping the operation of the cutter head. Recognizing soil-to-rock transition zones in advance can help improve constructability by allocating cutters properly and operating the machine with caution.

3.4 Mixed Ground

Mixed ground indicates a ground condition combining more than two different types of grounds, which greatly affects TBM operation (Toth *et al.*, 2013). In particular, the excavation of soil-rock mixed ground at the tunnel face causes difficulty in maintaining the counter-face pressure because excavating soil is relatively easier than excavating rocks, and an unbalanced over-excavation of soil can occur. The impact of cutters at the boundary line dividing the soil and rocks results in a one-sided abrasion of the cutters, leading to an increase in the consumption of cutters. Therefore, anticipating the distance for which the TBM will run is very important because excavating soil-rock mixed ground for a long time accelerates cutter damage and lowers the efficiency of excavation by increasing the TBM stand-up time. In general, TBM operators at most of the sites just go through temporarily emerged soil-rock mixed ground with caution because changing cutters can take more time than the time delay that results from the inefficiency of excavation. However, in the gradually emerging mixed ground for a long distance, as the TBM drives into the soil-to-rock transition zone, installing suitable cutters in the early stage can increase tunneling efficiency. In conclusion, mixed ground is one of the most disadvantageous ground conditions for mechanized tunnel construction. An idea of how long the TBM runs into the mixed

ground will be beneficial, allowing the operator to take necessary measures by reducing the rotation speed of the cutter-head and the thrust force.

3.5 Other Disadvantageous Ground Conditions

In addition to the hazardous ground conditions described above, several other problematic ground conditions are encountered during mechanized tunnel construction. For example, there may be cohesive clay layers that can increase the torque considerably or disturb the conveyance of excavated muck. The ground where core stone or boulder is present also involves potential risks that can damage cutters and the conveying system. Additionally, squeezing ground or swelling ground (with time) can be disadvantageous for construction.

In the preceding sections, hazardous ground conditions that can degrade the overall safety of the tunnel or decrease the construction efficiency are described. We can conclude that prediction of fractured zones, seawater bearing zones, soil-to-rock transition zones, and mixed ground in the early stages will be beneficial for improving constructability. In the next two sections, experimental studies for the advancement of TBM toward the afore-mentioned hazardous ground conditions are simulated in laboratory-scale tests. Subsequently, the advantages of using resistivity along with IP for distinguishing the types of hazardous ground conditions are discussed.

4. Experimental Preparation

4.1 Test Apparatus, Materials, and Equipment Settings

A tank of 50 cm length, 50 cm height, and 20 cm width is prepared to model laboratory-scale hazardous ground conditions (Fig. 5). The tank is made of 1.5-cm thick non-conductive polycarbonate; the upper and lower parts of the tank can be separated so that a ground condition can be easily constructed. Sandstone is used to model the bed rock and is placed at the bottom of the tank with a height of 23 cm, which is deep enough to avoid the boundary effect. In addition, to model jointed rock, sandstone is also cut into small pieces of identical sizes (3 cm × 3 cm × 20 cm). Clay, sand, and gravel are used to model the fractured ground as well as soil layers. The porosities (n) of the clay, sand, and gravel are 0.538, 0.411, 0.436, respectively. The rock and soils used in this experiment are saturated with tap water or seawater for more than 24 hours. The seawater with 35‰ salinity is prepared by adding sun-dried salt to distilled water. A cylindrical metal rod having a diameter of 1 mm is used as the electrode, and the Wenner electrode array with the electrode spacing of a = 6 cm is used to measure the resistivity and IP values.

To observe the boundary effect on the current flow, the tank was filled with tap water and the electrodes were moved from the center to the parallel and normal directions, respectively, by 1 cm in each test to measure the resistivity at each location of the electrode. The experimental results show that the resistivity is almost constant as the electrodes initially move from the center, however, the resistivity then gradually increases as the electrodes move closer to the boundary (in both parallel and normal directions), indicating that the current flow is influenced by the boundary effect only if the electrodes move closer to the boundary. Therefore, the boundary effect is negligible when the electrodes are located at the center of the tank.

The Supersting R8/IP (manufactured by Advanced Geoscience Inc.) was used to measure the DC resistivity and chargeability values. During the experiments, the measurement was performed at least 5 times for the same test to check the duplicability. Considering this was a small laboratory-scale test, the maximum current flow was set to 200 mA and the measurement duration of the decaying electric potential was set to 2 s. The total IP was recorded as the chargeability value.

4.2 Experimental Cases

Laboratory experiments were performed with four cases modeling the hazardous ground conditions: fault zone, seawater bearing zone, soil-to-rock transition zone, and mixed ground (refer to Table 1). In case 1, which models fault zone within the tank,

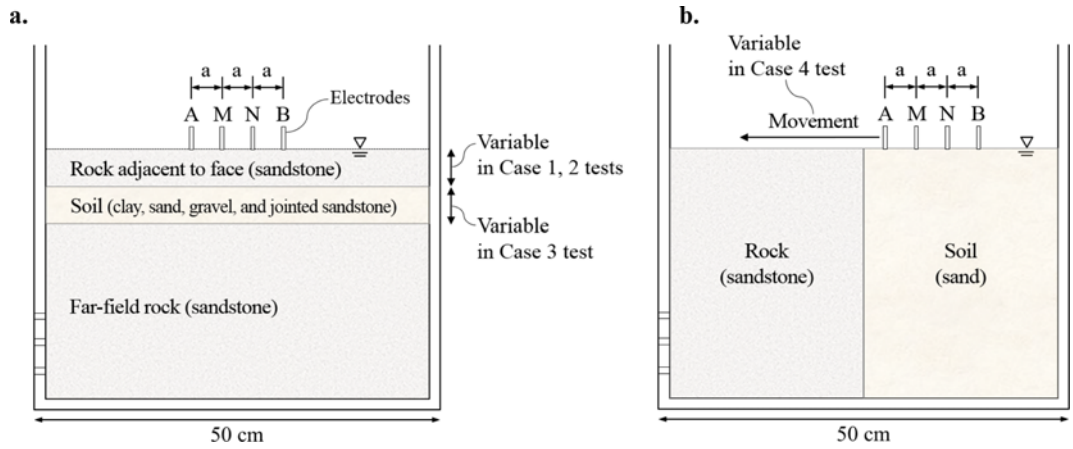

Fig. 5. Test Apparatus for Modeling the Hazardous Ground Conditions: (a) Fault, Seawater Bearing, and Soil-to-rock Zone, (b) Mixed Ground

Table 1. Experimental Cases: Modeling the Hazardous Ground Conditions Ahead of the TBM

	Case 1	Case 2	Case 3	Case 4
Risky ground type	Fault zone	Seawater intruded zone	Soil-to-rock transition zone	Mixed-ground Zone
TBM advancement modeling	Decrement of thickness of surface sandstone		Decrement of thickness of soil	Movement of four-electrodes
Ground materials	Sandstone, clay, sand, gravel, and jointed sandstone	Sandstone and gravel	Sandstone, clay, sand, and gravel	Sandstone and Sand
Pore water	Tap-water	Seawater	Tap-water	
Electrode array	Wenner array ($\overline{AM} = \overline{MN} = \overline{NM} = 6$ cm)			
Measured data	Direct current (DC) electrical resistivity and chargeability (time domain IP for 2 s)			

various forms of 3-cm high fractured layers were constituted by using jointed rock or different types of soil, such as clay, sand, and gravel (Fig. 5(a)). The surface and bottom sandstones represent rocks adjacent to the tunnel face and at the far field, respectively. The measurement of resistivity and IP at the surface rock, as the thickness of the surface rock is gradually decreasing, simulates the exploration procedure at the tunnel face during TBM advancement toward a fault zone. The case 2 test that modeled a seawater bearing zone was conducted under seawater level, and used gravel to model the fractured/weathered ground where seawater intrudes. In the case 3 test, surface sandstone was eliminated, and four-electrodes were installed in the soil layer (clay, sand, and gravel) overlaying the sandstone. The IP and resistivity were measured by decreasing the thickness of the soil layer so that the TBM's approach toward the soil-to-rock transition zone could be simulated. The case 4 test that models soil-rock mixed ground was carried out differently (see Fig. 5(b)). We filled the tank with sand and sandstone half-and-half (modeling the mixed ground) and moved the four electrodes from the sandstone zone to the sand zone. This procedure models the rise of the boundary line dividing the soil and rocks on the tunnel face as the TBM runs into soil-rock mixed ground. The four experimental cases are summarized in Table 1.

By the way, experiments were performed twice for each case and both experimental results showed an identical trend of changes in the measured resistivity and IP values as TBM advances. In the following chapter, the experimental results are presented with a normalized form.

5. Laboratory-scale Experiments

The effectiveness of using the IP method along with electrical resistivity for predicting hazardous grounds ahead of the tunnel face was evaluated in laboratory-scale experiments. As the TBM advances toward the hazardous ground, the resistivity and IP are assumed to be measured at the tunnel face using four electrodes installed at the cutter head whenever the excavation is stopped to assemble one ring of a segmental lining. In general, assembling one ring of a segmental lining by skilled engineers takes approximately thirty minutes. We expected the measurement of the resistivity and IP using electrodes installed at the cutter head to take around two minutes so that the implementation of the proposed resistivity and IP method, while the TBM was stopped to assemble the lining, would be

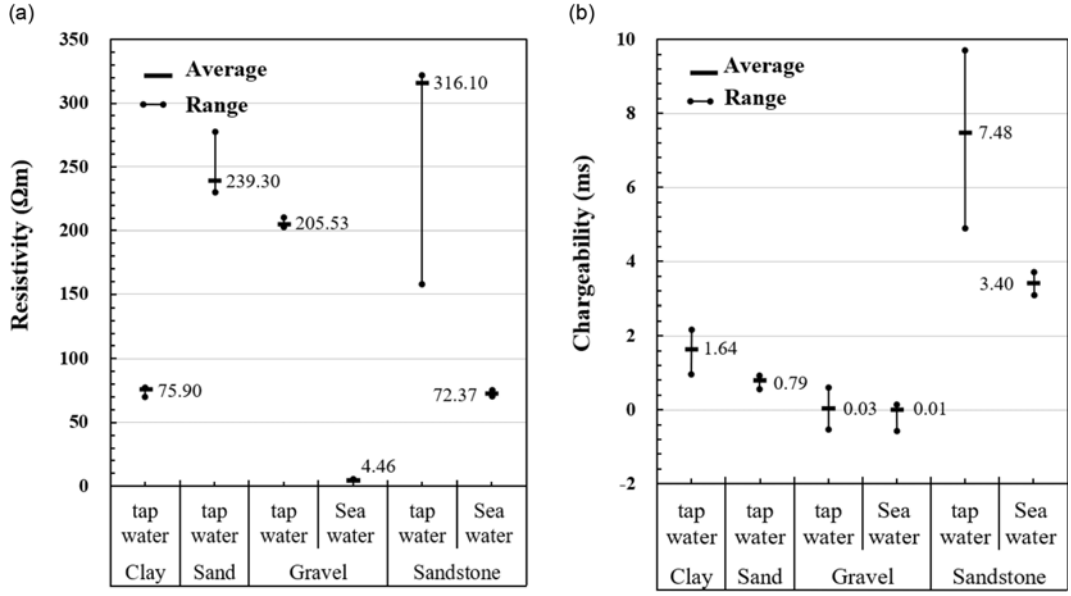

Fig. 6. Measured Values of: (a) Resistivity, (b) Chargeability

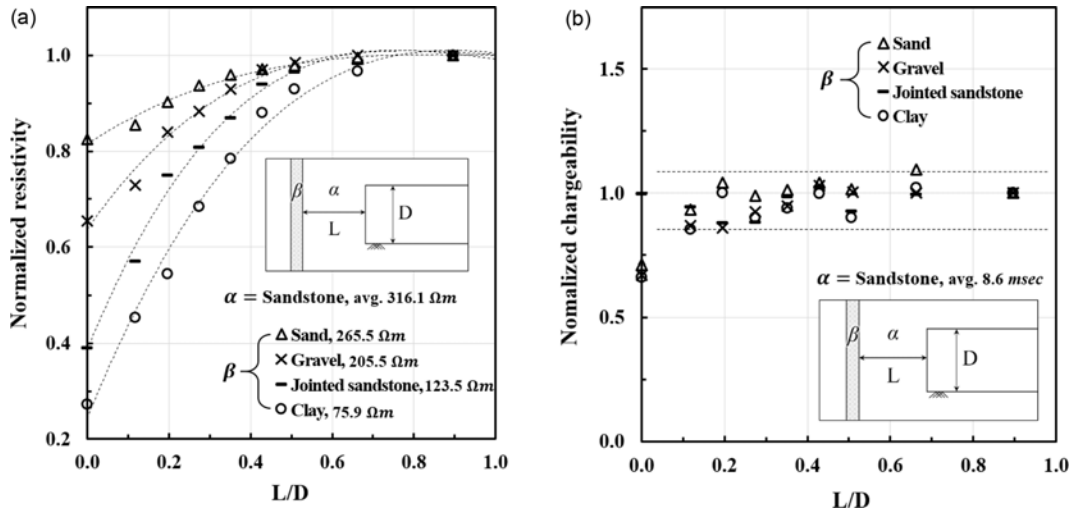

Fig. 7. Variation in the Resistivity and IP as the TBM Approaches a Fault Zone: (a) Normalized Resistivity, (b) Normalized Chargeability

practical and effective.

5.1 Characteristics of Soils and Rock

Firstly, the ranges of the measured resistivity and IP values of the clay, sand, gravel, and sandstone, which are used to model the ground conditions, are shown in Fig. 6. The measurements of all the materials are taken under the tap-water saturated condition, where the resistivity is 61.13 Ωm. In addition, the measured values of the gravel and sandstone under the seawater saturated condition, where the resistivity is 2.23 Ωm, are presented as well. The Wenner electrode array with a = 6 cm is used and three samples per each material are prepared to check the repeatability of the measured values among samples.

Among the materials saturated with tap water (see Fig. 6(a)), clay exhibits the lowest resistivity values, whereas, the resistivity of sandstone shows the highest value because the porosity (n) of sandstone is much lower than that of soils; clay, sand, and gravel. Moreover, when the materials are saturated with seawater, the measured resistivity decreases as the resistivity of the pore water (ρ_w) decreases (refer to Eq. (1)).

Meanwhile, the chargeability of both the sand and gravel are very small and close to 0 ms (the highest chargeability value is 0.8 ms); on the other hand, clay exhibits a marginally higher chargeability value (average value of 1.6 ms) as compared to those of sand and gravel. Moreover, the chargeability of sandstone is greater than that of soils (average value of 7.5 ms). This is because the radius of the narrow pore (r_1) of sandstone is much smaller than that of soils, so that cations are likely to accumulate in the small pore throat, resulting in higher chargeability. Furthermore, it can be inferred that the relatively larger range of chargeability values of sandstone might be due to the scattering of the narrow pore sizes of the sandstone itself. Additionally, the chargeability tends to decrease when materials are saturated with seawater, and this matches well with the results of sensitivity analysis on the IP mentioned in section 2.4, which demonstrates that the chargeability tends to decrease when the salinity of pore water (C_0) increases.

5.2 Influence of Fault Zones (Case 1)

Generally, fault gouge, fractured rock, and breccia are developed within a fault zone and can consist of clay, breccia cemented by clay or sand, and jointed zone depending on the degree of shear failure. Therefore, in this experiment, clay, sand, gravel, and jointed sandstone were used to model the various compositions of a fault zone layer that has higher porosity compared to intact sandstone. A TBM approaching a fault zone is simulated in the laboratory by reducing the thickness of the rock adjacent to the face as shown in Fig. 6(a). The measured resistivity and IP are normalized by using the measured values of resistivity and IP in the absence of a fault zone. The distance (L) of a fault zone from a tunnel face is also normalized by the tunnel diameter (D). The results are shown in Fig. 7.

Figure 7(a) shows that the resistivity value continuously decreases as the TBM approaches the fault zone; the decreasing tendency is more dominant when the fault zone is composed of jointed sandstone (simulating the fractured zone) and/or clay.

On the other hand, Fig. 7(b) shows that the IP value remains almost constant, even as the TBM approaches the fault zone. This is attributable to the radius of the narrow pore (r_1) of sandstone adjacent to the tunnel face, which is smaller than that of sand, gravel, and clay. The measured chargeability is mostly controlled by the ground that has the smallest narrow-pore (Park *et al.*, 2017b). When the tunnel face finally touches the fault zone, so that the ground adjacent to the tunnel face becomes a fault zone ($L/D = 0$), we can observe that the measured chargeability decreases, as the chargeability of soils (sand, gravel, and clay) controls the measured chargeability, beside the jointed sandstone case. The chargeability of jointed sandstone appeared to be identical to that of sandstone because joints do not influence the chargeability.

From these results, we can infer that the existence of a fault zone

ahead of a tunnel face in an actual tunnel construction site can be anticipated if the resistivity decreases while the IP remains almost constant, as the TBM advances toward the fault zone.

5.3 Influence of Seawater-bearing Zone (Case 2)

In this experiment, a fault zone, representing one of the poor ground conditions where seawater can intrude, was artificially modeled using gravel and the ground was saturated with seawater to create a seawater-bearing zone. Similar to the case 1 test, this experiment also simulates the advancement of the TBM toward the seawater-bearing zone by reducing the thickness of rock adjacent to the face. The experimental results are presented along with the result of the case 1 experiment, in which the fault zone is comprised of gravel under the tap-water saturated condition (see Fig. 8). Absolute values as well as normalized values are presented to evaluate the effect of seawater on the measured resistivity and IP, compared to the corresponding values for tap water.

Figure 8(a) shows that the resistivity value is much smaller when the ground is saturated with seawater, compared with the tap-water saturated condition, as the resistivity of pore water (ρ_w) decreases significantly under the seawater saturated condition (refer to Eq. (1)). When we examine the normalized resistivity (Fig. 8(b)), the normalized resistivity value decreases more steeply under seawater saturated condition than under tap-water saturated condition. In other words, the rate of decrease in resistivity under the seawater saturated condition is higher than that under the tap-water saturated condition, as the TBM approaches a fault zone.

Figure 8(c) also shows that the chargeability has smaller values with seawater saturation compared to tap-water saturation, as seawater causes the pore water concentration (C_0) to increase, which results in the lower chargeability. On the other hand, Fig. 8(d) shows that the IP value remains almost constant, even as the TBM approaches the fault zone. As mentioned earlier, this occurs as the chargeability of the sandstone adjacent to the tunnel

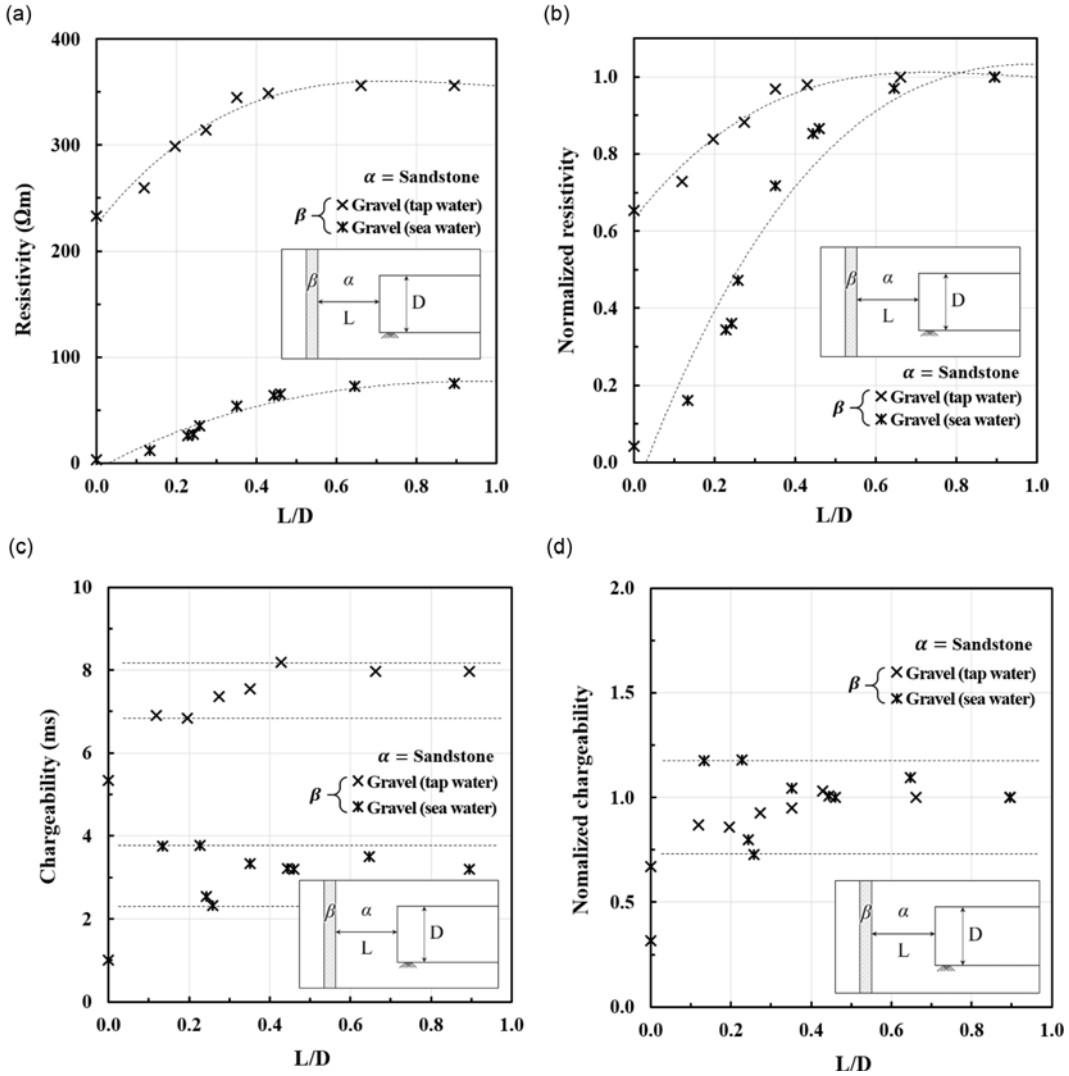

Fig. 8. Variation in the Resistivity and IP as the TBM Approaches to Seawater Bearing Zone: (a) Resistivity; (b) Normalized Resistivity, (c) Chargeability, (d) Normalized Chargeability

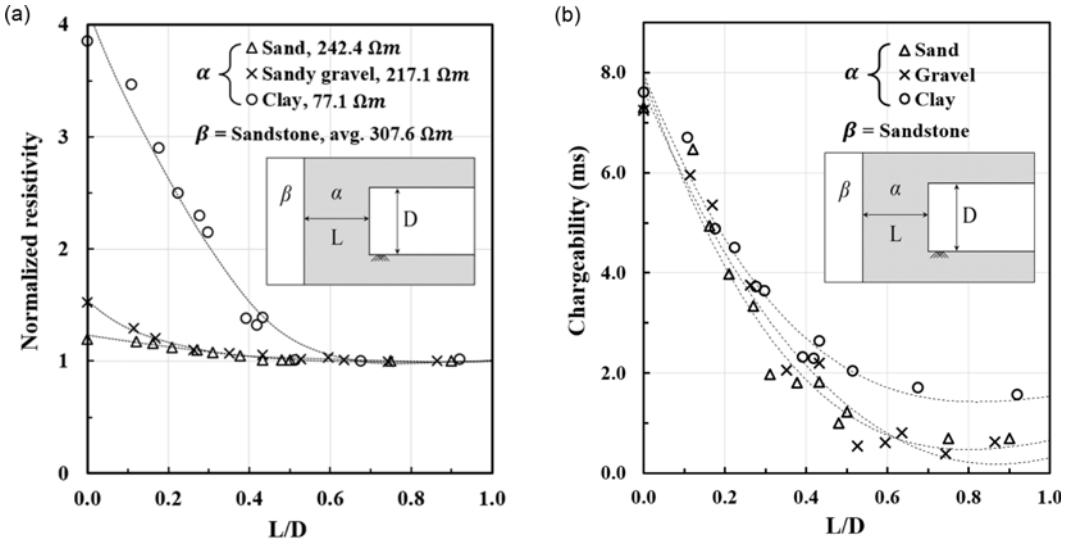

Fig. 9. Variation in the Resistivity and IP as the TBM Approaches the Soil-to-rock Transition Zone: (a) Normalized Resistivity, (b) Chargeability

face controls the measured chargeability even in the seawater saturated condition, and the chargeability decreases when the tunnel face touches the fault zone ($L/D = 0$).

In summary, we can observe that the trend of changes in resistivity and IP as the TBM approaches a fault zone is similar both in tap-water and seawater conditions; while absolute values appeared to be much smaller with the seawater saturated condition. This indicates that using absolute values as a reference for predicting the ground condition would also be useful. Moreover, the decreasing rate of resistivity as the TBM approaches the fault zone is more dominant in the seawater saturated condition compared to the tap-water saturated condition, which means an easier prediction of the fault zone saturated with seawater.

5.4 Influence of Soil-to-rock Transition Zone (Case 3)

A laboratory-scale experiment was also performed to simulate the advancement of a soil-excavating TBM toward rock ahead of the tunnel face. The resistivity and IP were measured by placing four electrodes directly on top of the soil, and the excavation procedure was modeled by reducing the thickness of the soil (refer to Fig. 5(a)). The measured resistivity is normalized by the resistivity of the soil. The results are shown in Fig. 9(a). However, since the IP of soils exhibits a very small value (close to 0 ms), the chargeability is presented as the absolute value, as shown in Fig. 9(b).

As shown in Fig. 9(a), the resistivity increases as the tunnel face approaches a rock since the rock has higher resistivity than soils. However, the increasing trend is not as significant as the TBM currently excavating soils approaches the rock, except for the case of transition from clay to rock. The resistivity tends to increase at a greater rate only when there is a greater difference between the resistivity value of the currently excavated soil and that of rock ahead of the tunnel face. This result suggests that it would be not easy to predict the transition of a soil-to-rock zone by utilizing only the resistivity value.

Meanwhile, Fig. 9(b) shows that the measured chargeability rapidly increases as the tunnel face approaches a rock zone, since a rock has a relatively higher chargeability than that of soils. This is because the radius of the narrow pore (r_1) of soil is much larger than that of a rock. Unlike case 1, in which the IP effect is mainly controlled by the rock adjacent to the tunnel face, the chargeability steadily increases as the thickness of soil decreases, and thus the distance between the electrodes and rock zone decreases (see Fig. 5(a)). Moreover, Fig. 9(b) shows that the increasing trend in the IP value, as the tunnel face approaches the rock zone, is applicable regardless of soil types.

From this result we can infer that observing the IP can be very useful in identifying a rock zone ahead of a tunnel face during soil excavation, even if the resistivity values of the rock and soil exhibit a minimal difference.

5.5 Influence of Soil-rock Mixed Ground (Case 4)

Mixed ground, which consists of both rock and soil on the tunnel face, was modeled in this laboratory-scale experiment. More specifically, the effect of the increase and/or decrease of the bottom rock layer on the measured resistivity and IP value with the advancing TBM is investigated, as shown in Fig. 10, to figure out how long the mixed ground condition will continue. To simulate the moving soil-rock boundary line on the face where the four electrodes are installed, we moved the electrodes continuously on the soil-rock mixed ground from the sandstone zone to the sand zone (see Fig. 5(b)).

The experimental results for the normalized resistivity show that the resistivity value decreases in the early stage, but begins to increase and then decreases again, when the soil-rock boundary line passes through the location of the potential electrodes M and N. In other words, the fluctuation of resistivity can be observed as the potential electrodes encounter the boundary line. This

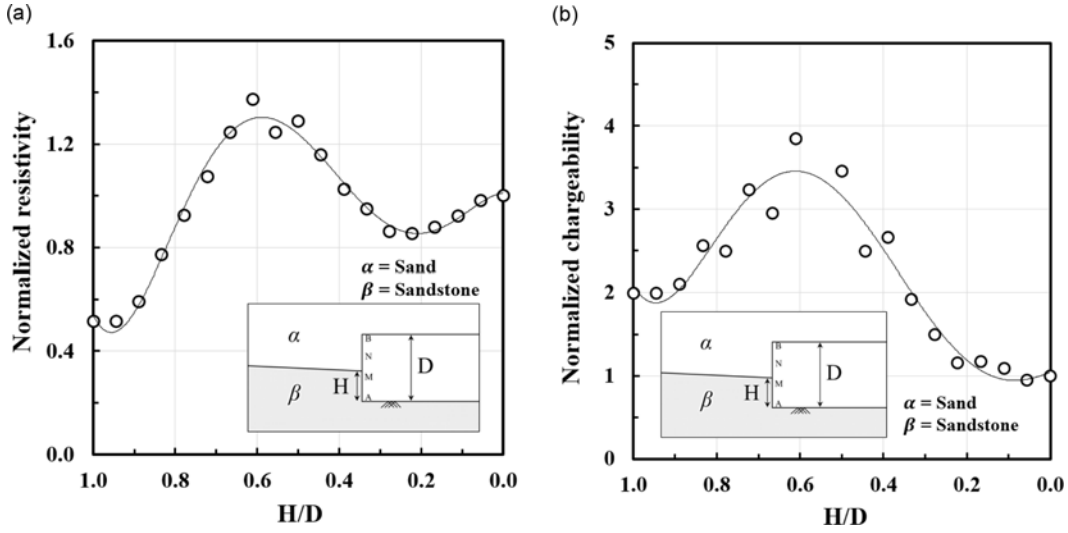

Fig. 10. Variation in the Resistivity and IP as the TBM Excavates Mixed Ground, so That Soil-rock Boundary Line Increases: (a) Normalized Resistivity, (b) Normalized Chargeability

phenomenon can be observed in the conventional resistivity survey as well, which is performed on the ground surface when the potential electrodes are located on the boundary dividing two different grounds exhibiting different resistivity values. Furthermore, the cause of such resistivity fluctuation was identified theoretically. Separate governing equations for estimating the electric potential were derived between the electrode A and M, M and N, and N and B, respectively, which resulted in such peaks and troughs in resistivity, because different electric potentials will eventually lead to different electrical resistivities (Van Nostrand and Cook, 1966).

Meanwhile, the measured IP value also shows fluctuations as the TBM excavates soil-rock mixed zone. The IP gradually increases at the beginning and then decreases when the second potential electrode N encounters the boundary line. These changes in chargeability also seem to result from the afore-mentioned governing equation that controls the changes in the electric potential, since the IP value is the outcome of the decreasing electric potential. Choi *et al.* (2008) also obtained similar results when they measured the IP values on the ground surface composed of a sand-clay mixture.

In summary, as the bottom rock layer increased adjacent to the tunnel face, the IP increased gradually; the resistivity initially decreased and increased again at the location of the electric potential M. Subsequently, both the resistivity and IP decreased once the boundary line touched the potential electrode N.

6. On-site Prediction Guide utilizing the Proposed Method

In the previous section, four different types of risky grounds (cases 1, 2, 3, and 4) were artificially modeled, and variations of the measured resistivity and IP, as the TBM approaches a hazardous ground, were observed in laboratory-scale experiments. In this section, the utilization of the characteristics of the variations in the resistivity and IP for identifying risky ground in advance will be discussed. The experimental results are summarized in Table 2, which shows the variation of the measured resistivity and IP at a glance, as the TBM advances toward each type of hazardous ground.

If we assume a gradual decrease in the measured resistivity value as the TBM runs, the exact cause of such reduction in resistivity cannot be clearly identified, because it could have

Table 2. Variation of resistivity and IP as the TBM advances toward hazardous ground conditions

Risky grounds / Measurement	Fault zone (Case 1)	Seawater bearing zone (Case 2)	Soil-to-rock transition zone (Case 3)	Soil-rock mixed ground (Case 4)
	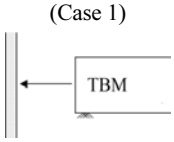	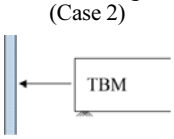	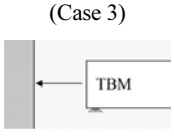	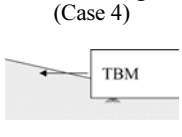
Electrical resistivity	Decrease ↓	Decrease ↓	Increase ↑	Fluctuate ↓↑
Chargeability (IP)	Constant →	Constant with small value →	Increase ↑	Fluctuate ↑↓
Note	The ground is saturated with tap-water	Much lower values are measured compared to case 1	Resistivity increases only when the resistivity of the rock is much larger than that of the soil	

been caused either by a fault zone with high porosity (n) that exists ahead of the tunnel face, or by the decrease in the resistivity of (ρ_w) pore water in the ground (refer to Eq. (1)). However, the cause of the decrease in resistivity can become clearer when changes in the IP are also examined. We can say that the decrease in the resistivity is caused by the poor condition of the ground rather than the change in the resistivity of pore water (or change in the concentration of pore water) if the measured IP appears to be constant during excavation, since the IP is not affected by the fracture characteristics of the ground ahead of the tunnel face. On the contrary, if both the resistivity and IP start to gradually decrease together during excavation, we can say that the decrease in the pore-water resistivity (increase in concentration of pore water) is the main cause of such a phenomenon. This is because the concentration of pore water (C_0) is one of the factors influencing the IP; the increase in the pore-water concentration results in a decrease in the IP. Therefore, we can say that the IP exploration results can be a useful tool for identifying the presence of a fault zone during tunneling works in urban areas or under the sea.

Meanwhile, a rock zone can appear ahead of the tunnel face when both the resistivity and IP gradually increase during the excavation of soil (see case 3 in Table 2). However, as the experimental results showed that the resistivity increased only when the relative difference in the resistivity of excavating soil and that of the rock ahead of the tunnel face is significant, this in contrast, means that predicting the rock ahead of the tunnel face by observing the changes in the resistivity alone can be difficult when there is minimal difference between the resistivity of soil and that of rock. Further, sedimentary rocks like shale, sandstone, and siltstone with high porosity can show lower resistivity than soil (James and Richard, 2011), which reveals the limitation of the resistivity survey. On the other hand, in the case of the IP, the chargeability of sandstone showed a range of 5.0 ~ 9.7 ms, which appeared to be much higher than the chargeability of soil which showed a maximum value of 2.2 ms in our experiments (refer to Fig. 6(b)). In addition, Telford *et al.* (1990) explained that rocks in general showed higher IP than soil as alluvium had a chargeability range of 1 ~ 4 ms, while schists and sandstone had chargeability ranges of 5 ~ 20 ms and 3 ~ 12 ms, respectively. Therefore, we can say that the IP effect of rock appears to be higher than that of soil in general. This is caused by the particles in the rock, which are arranged more compactly (densely packed) than soil particles, resulting in a high cation concentration and high chargeability, enabling us to distinguish between soil and rock using the IP method. Hence, we can conclude that the IP method will be effective in predicting the existence of rock ahead of the tunnel face during soil excavation.

The last scenario is about entering a soil-rock mixed zone where rocks gradually appear in muck. As mentioned earlier, identifying the extent of the mixed ground to be excavated is important. As the TBM enters a mixed zone, the resistivity will begin to decrease and increase thereafter, while the IP steadily increases as the boundary between the rock and soil layer moves upward, until it touches the potential electrode M. By examining these changes we can expect the excavation of mixed ground to continue until the boundary continuously moves up, when both the resistivity and IP switch back to a decreasing trend as the rising bedrock gradually occupies the tunnel face.

On the other hand, the scale effect between the laboratory scale and the field scale should be noted. The experimental model presented in this paper simulates the resistivity exploration at mechanized-tunneling job site with 1/30 reduced size, in which electrode of 30 mm diameter and the widest electrodes spacing of 5,500 mm are used for exploration (refer to Park *et al.*, 2017b). Nevertheless, the ground prediction using electrical methods is based on observing the trend of changes in the measured resistivity and IP values resulting from the changes of ground conditions, as a TBM advances. Therefore, the proposed prediction guide, which uses the variation trend of the resistivity and IP values, will also be applicable to real tunnelling sites. Furthermore, if we observe the overall trend of the resistivity and IP values, the combined method of using resistivity and IP survey simultaneously might also be a proper method for predicting the risky ground condition, even in the field composed of non-homogeneous rocks and/or soils (Park *et al.*, 2017a; Park *et al.*, 2017b).

Moreover, as a further research, if the resistivity and IP data can be gathered from the mechanized-tunnelling job sites along with the information of the actual ground conditions as a TBM runs, a more reliable and efficient prediction method can be achieved if a noble statistical method is used for the acquired data from the sites, such as a stochastic approach based on artificial neural network (Hamdia *et al.*, 2015).

7. Conclusions

This study verifies the effectiveness of using both the Induced Polarization (IP) and electrical resistivity for predicting hazardous ground conditions ahead of a mechanized tunneling face by conducting laboratory-scale experiments. The advantages of using the IP in addition to the resistivity for identifying different types of hazardous ground conditions are mainly studied in this paper. The conclusions drawn from this study are summarized as follows:

1. During TBM tunneling, in coastal areas or under the sea where either seawater or fresh water exist depending on the ground condition, the exact cause of the decrease in the resistivity as the TBM advances is not clear because it is difficult to distinguish whether it results from the high porosity of a fault zone that is located in front of the TBM, or from the increased concentration of pore water by seawater intrusion. However, since the IP decreases as the pore-water concentration increases and it is not controlled by the fracture characteristics of the rock ahead of the tunnel face, using the IP value to identify the exact cause of the resistivity decrement is feasible. Thus, a more reliable prediction of a fault zone ahead of the tunnel face can be achieved by using the IP and resistivity methods together in areas susceptible to

seawater intrusion. Moreover, since performing surface-based geological investigations is restricted in the sea, the demand for the proposed resistivity and IP method that can be implemented inside the tunnel would be high in subsea tunneling job-sites.

2. In the prediction of the rock ahead of the tunnel face when excavating soils, using resistivity is considered useful only when there is a significant difference in the resistivity value between the soil and rock, causing a steep increase in the resistivity as the TBM approaches the rock. This implies that predicting the rock ahead of the tunnel face may not be easy when the resistivity values of the soil and rock do not differ significantly. However, the IP of a rock generally exhibits much higher values than that of soils because the rock has more densely packed particles than soils resulting in a higher cation concentration. Thus, the IP method can remedy the shortcoming of the resistivity method for detecting the rock zone in front of the TBM concurrently, when excavating soils.
3. The combined measurement of the IP and resistivity is a good means to predict the extent of the mixed ground ahead of the tunnel face. As the bottom rock layer of the mixed ground increases (moves up) adjacent to the tunnel face, the IP increases gradually; the resistivity initially decreases and increases again. Both the resistivity and IP decrease as the rock layer keeps moving up. We can thus predict how long the TBM will have to run into the mixed ground by observing such fluctuations in the measured resistivity and IP values during tunnel excavation by TBMs.
4. Lastly, the electrodes installed for the resistivity survey can also be used for the IP exploration; no additional efforts are needed. The resistivity and IP measurement takes only about two minutes. Therefore, implementing the IP survey along with the resistivity, whenever the excavation is stopped to assemble one ring of a segmental lining, will be highly effective and practical in mechanized-tunneling job sites.

Acknowledgements

This research was supported by a grant (Project number: 13SCIP-B066321-01 (Development of Key Subsea Tunneling Technology)) from the Infrastructure and Transportation Technology Promotion Research Program funded by the Ministry of Land, Infrastructure and Transport of the Korean government. The corresponding author thanks Korea University for granting him sabbatical leave in order to concentrate on this research.

References

Archie, G. E. (1942). "The electrical resistivity log as an aid in determining some reservoir characteristics." *Trans. Am. Inst. Min. Metall. Eng., Society of Petroleum Engineers*, Vol. 146, No. 1, pp. 54-62, DOI: 10.2118/942054-G.

Chang, S. H., Bae, G. J., Jeon, S., Yu, Y. I., and Oh, S. J. (2006). "Risk management in a TBM Tunnel." *13th Tunnel Committee Special Conference*, KSCE, Seoul, Korea, pp. 91-114 (in Korean).

Cho, G. C., Choi, J. S., Lee, G. H., and Lee, J. K. (2005). "Prediction of ground-condition ahead of tunnel face using electric resistivity-analytical study." *Proc. of Int. World Tunnel Cong.*, AITES-ITA, Istanbul, Turkey, pp. 1187-1194.

Choi, S., Kim, H. S., and Kim, J. S. (2008). "IP characteristics of sand and silt for investigating the alluvium aquifer." *J. Engng. Geol.*, Vol. 18, No. 4, pp. 423-431 (in Korean).

Dickmann, T. and Sander, B. K. (1996). "Drivage-concurrent Tunnel Seismic Prediction (TSP): Results from Vereina north tunnel mega-project and Piora pilot gallery." *Geomechanik-Kolloquium*, Vol. 14, No. 6, pp. 406-411.

Grodner, M. (2001). "Delineation of rockburst fractures with ground penetrating radar in the Witwatersrand basin, South Africa." *Int. J. Rock Mech. Min. Sci*., Vol. 38, No. 6, pp. 885-891, DOI: 10.1016/S1365-1609(01)00054-5

Hamdia, K. M., Lahmer, T., Nguyen-Thoi, T. and Rabczuk, T. (2015). "Predicting the fracture toughness of PNCs: A stochastic approach based on ANN and ANFIS." *Computational Materials Science*, Vol. 102, pp. 304-313, DOI: 10.1016/j.commatsci.2015.02.045

James, A. and Richard, P. (2011). "Inexpensive geophysical instruments supporting groundwater exploration in developing nations." *J. Water Resour. Prot.*, Vol. 3, No. 10, pp. 768-780, DOI: 10.4236/jwarp.2011.310087.

Kaus, A. and Boening, W. (2008). "BEAM-geoelectrical ahead monitoring for TBM-drives." *Geomech. Tunn*., Vol. 1, No. 5, pp. 442-449, DOI: 10.1002/geot.200800048.

McDowell, P. W., Barker, R. D., Butcher, A. P., Culshaw, M. G., Jackson, P. D., McCann, D. M., Skipp, B. O., Matthews, S. L., and Arthur, J. C. R. (2002). *Geophysics in engineering investigations*, CIRIA, London, UK, pp. 61-185.

Morrow, C., Lockner, D. A., and Hickman, S. (2015). "Low resistivity and permeability in actively deforming shear zones on the San Andreas Fault at SAFOD." *J. of Geoph. Resear.*, Vol. 120, No. 12, pp. 8240-8258, DOI: 10.1002/2015JB012214.

Park, J., Lee, K. H., Kim, B. K., Choi, H., and Lee, I. M. (2017a). "Predicting anomalous zone ahead of tunnel face utilizing electrical resistivity: II. Field tests." *Tunn. Undergr. Space Technol.*, Vol. 68, pp. 1-10, DOI: 10.1016/j.tust.2017.05.017.

Park, J., Lee, K. H., Park, J., Choi, H., and Lee, I. M. (2016). "Predicting anomalous zone ahead of tunnel face utilizing electrical resistivity: I. Algorithm and measuring system development." *Tunn. Undergr. Space Technol.*, Vol. 60, pp. 141-150, DOI: 10.1016/j.tust.2016.08.007.

Park, J., Lee, K. H., Seo, H., Ryu, J., and Lee, I. M. (2017b). "Role of induced electrical polarization to identify soft ground/fractured rock conditions." *J. Appl. Geoph.*, Vol. 137, pp. 63-72, DOI: 10.1016/j.jappgeo.2016.12.017.

Reynolds, J. M. (1997). *An introduction to applied and environmental geophysics*, John Wiley & Sons, New York, N. Y., pp. 289-348.

Robert, A. (2014). *Forward probing ahead of tunnel boring machines*, AFTES recommendations GT24R2A1, French Tunnelling and Underground Space Association, Paris, pp. 132-169.

Schaeffer, K. and Mooney, M. A. (2016). "Examining the influence of TBM-ground interaction on electrical resistivity imaging ahead of the TBM." *Tunn. Undergr. Space Technol.*, Vol. 58, pp. 82-98, DOI: 10.1016/j.tust.2016.04.003.

Telford, W. M., Geldart, L. P., and Sheriff, R. E. (1990). *Applied geophysics, second ed.*, Cambridge University Press, New York, N. Y., pp. 578-

609.

Titov, K., Kemna, A., Tarasov, A., and Vereecken, H. (2004). "Induced polarization of unsaturated sands determined through time domain measurements." *Vadose Zone Journal*, Vol. 3, No. 4, pp. 1160-1168, DOI: 10.2113/3.4.1160.

Toth, A., Gong, Q., and Zhao, J. (2013). "Case studies of TBM tunnelling performance in rock-soil interface mixed ground." *Tunn. Undergr. Space Technol.*, Vol. 38, pp. 140-150, DOI: 10.1016/j.tust.2013.06.001.

Van Nostrand, R. G. and Cook, K. L. (1966). *Interpretation of resistivity data*, U.S. Government Printing Office, Alexandria, Washington, USA, pp. 45-55.

Vlasov, S. N., Makovsky, L. V., and Merkin, V. E. (2001). *Accidents in transportation and subway tunnels: Construction to operation*, Elex-KM Publ. Ltd, Moscow, Russia, pp. 17-87.

Vu-Bac, N., Lahmer, T., Zhuang, X., Nguyen-Thoi, T., and Rabczuk, T. (2016). "A software framework for probabilistic sensitivity analysis for computationally expensive models." *Advances in Engineering Software*, Vol. 100, pp. 19-31, DOI: 10.1016/j.advengsoft.2016.06.005.